We are IntechOpen, the world's leading publisher of Open Access books Built by scientists, for scientists

6,900
Open access books available

185,000
International authors and editors

200M
Downloads

Our authors are among the

154
Countries delivered to

TOP 1%
most cited scientists

12.2%
Contributors from top 500 universities



WEB OF SCIENCE™

Selection of our books indexed in the Book Citation Index in Web of Science™ Core Collection (BKCI)

Interested in publishing with us?
Contact book.department@intechopen.com

Numbers displayed above are based on latest data collected.
For more information visit www.intechopen.com



Chapter

Monitoring Storm Impacts on Sandy Coastlines with UAVs

Alex Smith, Brianna Lunardi, Elizabeth George and Chris Houser

Abstract

UAV applications have shown the potential to increase the efficiency of collecting high resolution and spatially extensive topographic datasets of sandy coastal systems. These systems are dynamic and sensitive to variability in wave energy, evident in topographic adjustments associated with storm events. Topographic and volumetric changes of a beach-dune system were measured following a post tropical storm event. Using a pre-storm LiDAR and post-storm UAV survey, we identified high magnitude and continuous alongshore erosion of the foredune. Lower magnitude and discontinuous areas of deposition were also recorded, as sediment eroded from the foredune translated seaward and was deposited onto the beach. Overall, a total volumetric loss of ~11,000 m^3 from the beach-dune zone was recorded along the 2.5 km survey extent. Our results highlight the capability of UAVs for rapid monitoring and quantification of storm impacts. Furthermore, confidence in reported topographic changes was improved by implementing quality control measures and handling of data uncertainties (e.g., vegetation). The aim of this chapter is to quantify the impact of a storm event on a beach-dune system and discuss methodological challenges of monitoring sandy coastlines with UAVs.

Keywords: UAV applications for coastal monitoring, structure from motion, storm impacts, beach-dune interactions, dune recovery

1. Introduction

Sandy coastlines are dynamic environments that are continuously modified in response to wave, tidal, and eolian processes. Sediment is in constant flux amongst the nearshore, foreshore, and backshore (**Figure 1**). Over short time scales (i.e., hours to months), individual storm events and seasonal variability in wave and wind energy result in topographic adjustments [1]. For example, characteristic 'winter' or 'summer' profiles can develop where sediment movement between zones can be cyclically removed, stored, and/or returned [2, 3] (**Figure 1**). The 'winter' profile develops in periods of higher wave energy where sediment is removed from the backshore (i.e., through beach and foredune scarping) and stored in nearshore sand bars [2, 3]. As wave energy decreases, sediment can be returned landward through welding of nearshore sand bars onto the foreshore and deposition

IntechOpen

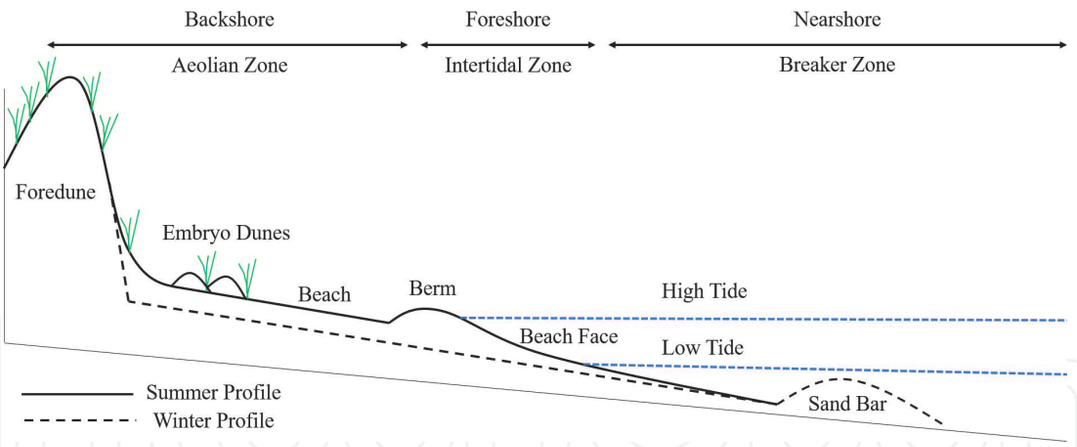


Figure 1.
This idealized diagram depicts the seasonal variability of across shore profiles, landforms, and vegetation that can develop during periods of increased (i.e., winter profile) or decreased (i.e., summer profile) wave energy.

of berm deposits on the beach [2, 3], leading to embryo dune development and foredune recovery [4] (e.g., 'summer' profile; **Figure 1**).

Small scale topographic variability is subsumed by larger scale controls on coastal dynamics [1, 5, 6] except in the presence of an alongshore variable framework geology [7]. However, changes in wave climate [8] and eustatic sea level [9] have the potential to disrupt the current balance between erosional and depositional processes. These climatic changes could lead to increased water levels during storm events and the potential for sediment to be transported inland through breaching [10, 11], overwash [12] or the development of blowouts [13, 14]. Sediment deposited landward of the foredune would be effectively removed from the cyclical 'seasonal' recovery state, and could lead to increased erosion, fragmentation, and landward retreat of the foredune [15, 16]. This disruption of sediment supply could also accelerate the transgression of the coastline as it responds to future changes in sea level [9]. Thus, the ability of foredunes to recover following storm events will have implications on both the short- and longer-term resiliency of sandy coastlines [17, 18].

Following significant storm events or storm seasons, periods of increased wave energy often leads to the development of a foredune scarp (**Figure 2**). The ability of the foredune to recover, or return to its pre-storm morphology, is then controlled primarily by the sequence and relationship between eolian transport potential and sediment supply [4]. Initially, sediment eroded from the foredune by elevated storm surge and wave run up can be deposited directly onto the beach or further seaward into nearshore bar structures [2, 3]. As the beach slope relaxes to a characteristic 'winter' or flattened beach profile (**Figure 2**), the low sloping surface promotes rapid boundary layer development during on shore winds and increases sediment flux potential [19], with minimal slope controlled limitations on flux magnitude [20]. Elevated wrack lines (**Figure 2**), exposed lag deposits, and large woody debris that may be present following storm events can temporarily trap sediment blown into the beach-dune boundary (e.g., see [6]).

Over seasonal or annual time scales, sediment stored in nearshore bars can begin migrating landward during periods of reduced wave energy [2, 3]. An increase in sediment supply into the foreshore can result in the formation of multiple berm ridges that are deposited above high tide and swash lines, increasing beach width [3]. This results in a larger supply of dry erodible sediment in the backshore which is less affected by tidal or swash driven surface moisture constraints on eolian transport [21]. Finally, vegetation recolonization at the beach-dune boundary can



Figure 2.
A foredune scarp observed at Brackley Beach, Prince Edward Island National Park, following the post-tropical storm Dorian in September 2019. This image shows that significant erosion of the stoss slope resulted in the formation of a steep and continuous scarp, alongshore. Other storm impacts, including a flattened across shore profile and elevated wrack line, are also visible.

limit transport potential and initiate dune building (e.g., [22]). If these conditions persist, dune recovery can occur through ramp building and embryo dunes can develop seaward of the established foredune [15]. Following major erosion events, full dune recovery may take years to complete [17, 23] and is controlled by frequency of high magnitude events [17].

The impact of a storm and the relatively slow recovery tend to be considered a two-dimensional, cross-shore phenomenon in which the storm impact depends only on the height of the storm surge relative to the elevation of the dune crest (e.g., [24, 25]). However, the foredune line is not uniform and can exhibit considerable variability in height, volume, and alongshore extent [12, 26, 27]. As noted, the exact location of dune erosion and overwash penetration depends on the correspondence of alongshore variations in the incident forcing and on existing gaps and low-lying areas along the dune line [28–31]. Understanding the variability of the beach-dune systems is essential to understanding the response of sandy coastlines to changes in storm activity and sea level rise, and it is important to the development of appropriate sampling strategies for field studies of sediment transport exchange amongst the nearshore, beach and dune (e.g., [31]).

Climatic change over the coming decades, including increased storminess [8] or sea level rise [9], have the potential to modify current beach-dune interactions. For example, an increased frequency of storm surge events can lead to barrier island systems of low elevation and discontinuous dunes that, in turn, increase the potential for island inundation and breaching [17]. However, a low frequency of storm surge can limit sediment transfer to the backbarrier as overwash leading to island drowning in response to an increase in sea level [32], unless sediment transfer is accomplished by blowouts [13, 14]. Monitoring the resiliency of sandy coastlines is, therefore, critical to our understanding on how these systems will respond to larger scale sedimentological and climatic perturbations. To address this challenge, advances in surveying technology including unmanned aerial vehicles (UAVs) and light detection and ranging (LiDAR) systems are able to provide robust geo-spatial data sets that will enhance repeat survey strategies of these dynamic environments.

1.1 Coastal applications for UAVs

The affordability and capability of UAV surveys to rapidly produce spatially extensive and high-resolution terrain models has been a boon to geoscientific research over the past decade (e.g., [33]). The majority of which has used Structure from Motion (SfM) photogrammetry. This technique generates automatic tie points (ATPs) between overlapping images and triangulates their position to produce a 3-D point cloud [34, 35]. The utility of UAVs and SfM have been well documented; however, difficulties remain in accurately capturing areas of topographic complexity, water boundaries, and vegetation [33]. The latter two can be particularly problematic in coastal environments due to variability in tidal ranges and/or wave run up on the seaward boundary [36, 37] and in the density of seasonally intermittent or established vegetation across the beach and foredune [38–41]. Other common problems that arise in coastal environments include wet or low texture surfaces that limit image recognition [41], maximum operational wind conditions of $\sim <$ 25 km/h [37, 42], and regulations that restrict UAV flights in the vicinity of pedestrians [37].

Due to these difficulties, the breadth of UAV research monitoring sandy coastlines has been relatively limited. Research testing the quality of SfM derived point clouds to those produced by more traditional methods such as terrestrial laser scanning (TLS) has found good agreement in areas with limited vegetation height or density [39, 41]. Furthermore, the geo-referencing of UAV point clouds using survey ground control points (GCPs) have been able to obtain centimeter scale error over non-vegetated surfaces [36, 38–40, 43]. However, the elevational error over vegetated surfaces can be an order of magnitude or higher, ranging from the 10–100-cm scale and is largely controlled by vegetation density and canopy height [41]. To date, only a small number of UAV coastal monitoring studies have quantified topographic or volumetric changes of beach-dune morphology in response to storm events [37], storm seasons and human management [38, 44], or annual cycles [40, 45].

UAV and SfM applications have displayed the potential to increase the efficiency and rapidity of coastal monitoring. In order for this potential to be fully realized, difficulties arising during data collection, processing, and analysis must be addressed when developing systematic and repeatable survey strategies. Recently, UAV coastal research have also used multi-spectral (e.g., [46]) and LiDAR sensors (e.g., [47]); however, this chapter will focus specifically on UAV and SfM systems. The remainder of this chapter will be an introduction to basic quality control measures, handling of survey and environmental uncertainties, and reporting of topographic and volumetric changes associated with a storm event. Furthermore, the persistent challenges of coastal monitoring with UAVs and prospective solutions will be discussed. Ultimately, the aim of this chapter is to present a repeatable methodology to confidently report topographic change and highlight future methodological advances that are still needed to improve upon current coastal monitoring strategies using UAVs.

2. Study site

Brackley Beach (BB; 46°25′50″ N 63°11′50″ W) is a part of the Prince Edward Island National Park, located on the north shore of Prince Edward Island (PEI), Canada (**Figure 3A**). BB extends ~6 km alongshore in an east to west orientation and is backed by a highly continuous foredune. On September 7th and 8th BB was impacted by the post-tropical storm Dorian (SD). Sustained N–NNE winds of up to

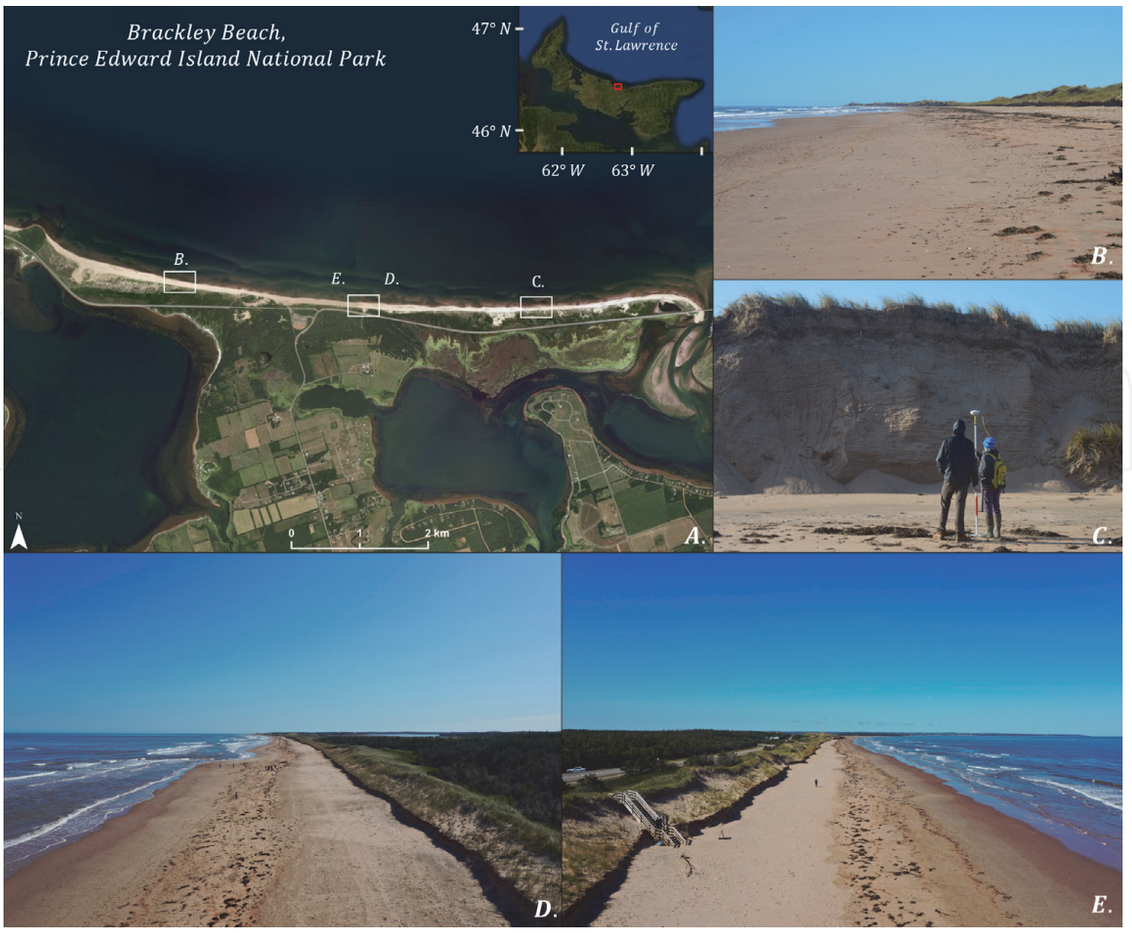


Figure 3.
Brackley Beach (A), Prince Edward Island National Park, extends ~6 km in an east to west orientation and is backed by highly continuous foredune. Following the storm Dorian, a flattened beach profile (B), significant foredune erosion (C), a continuous scarp developed alongshore (D and E).

55 km/h and gusts of up to 93 km/h were recorded at the Stanhope meteorological station (SMS), located ~9 km east of BB. It must be noted that SMS records wind conditions at 3 m above the surface, or 7 m below standard meteorological recordings, and likely underrepresent the peak wind speeds associated with SD. Additionally, there are no offshore buoys on the north coast of PEI to record marine conditions associated with SD; however, significant wave heights of 7–8 m and a storm surge of 1.2 m was forecasted by the Dalcoast-HFX model [48]. Peak storm surge levels, coincident with a ~0.8 m high tide recorded on the north coast of PEI at 2 a.m. on September 8th, are estimated to be ~2 m above mean sea level (MSL). An initial site assessment of SD's impact on BB observed modification of the beach-dune morphometry including a flattened beach profile (**Figure 3B**), scarping of the entire frontal slope (i.e., from the dune toe to dune crest) of the foredune at the eastern section of BB (**Figure 3C**), and a continuous 1–2 m scarp across the majority of the mid and western sections of BB (**Figure 3D** and **E**).

2.1 Pre-SD baseline survey

An integrated aerial LiDAR topographic and bathymetric (topobathy) survey was conducted at Prince Edward Island National Park between the 4th and 7th of July 2019. The LiDAR data was obtained through CBCL Limited with permissions from Parks Canada, as part of the Federal Transportation Risk Assessment Initiative. A Leica Chiroptera II dual sensor Topobathy LiDAR, utilizing an infrared (240 kHz) and green laser (35 kHz), seamlessly captured 291 m swaths of both the

topographic surface and near shore bathymetry, up to 5 m water depth. The survey was flown at an altitude of 400 m above the ground surface and maintained a sampling density of 2.72 points per meter (p/m) for the bathymetric and 18.6 p/m for the topographic surfaces. Point clouds were then geo-referenced using a total of 141 ground control points with a root mean square error (RMSE) of 0.05 m for the vertical transformation. The point cloud data was then classified for surficial and supra-surficial elements (e.g., vegetation, water surface, etc.). Following classification of the point cloud, only bathymetric and topographic surface classes were maintained to produce a 1 m × 1 m 'bare earth' or digital terrain model (DTM) that will serve as a pre-SD baseline for comparisons to post-SD UAV surveys.

3. Methodology

3.1 UAV survey design and initial SfM quality controls

On the 19th and 20th of September 2019, 11 days following SD, a survey consisting of eight overlapping UAV flight grids (**Figure 4A**) was flown at BB. Images were collected with a Mavic 2 Pro quadcopter and covered an alongshore extent of ~2.5 km. Across shore, UAV flight paths were programmed to capture images from the nearshore, foreshore, backshore, and back dune zones with 80% frontal- and 70% side-overlap. The UAV was flown at an altitude of 50 m corresponding to a ground sampling distance of ~1 cm/pixel. In each flight grid, at least 10 bright white bucket lids (30 cm in diameter) were used as GCPs and spread in a non-uniform placement across the foreshore, beach, and foredune (**Figure 4A**). The geographic location of each GCP was surveyed using a Global Navigation Satellite Series GPS. The high number of GCPs was designed to increase the accuracy of the geographic coordinate conversion by providing a diverse set of elevational references and to systematically build in redundancy that allow for GCP

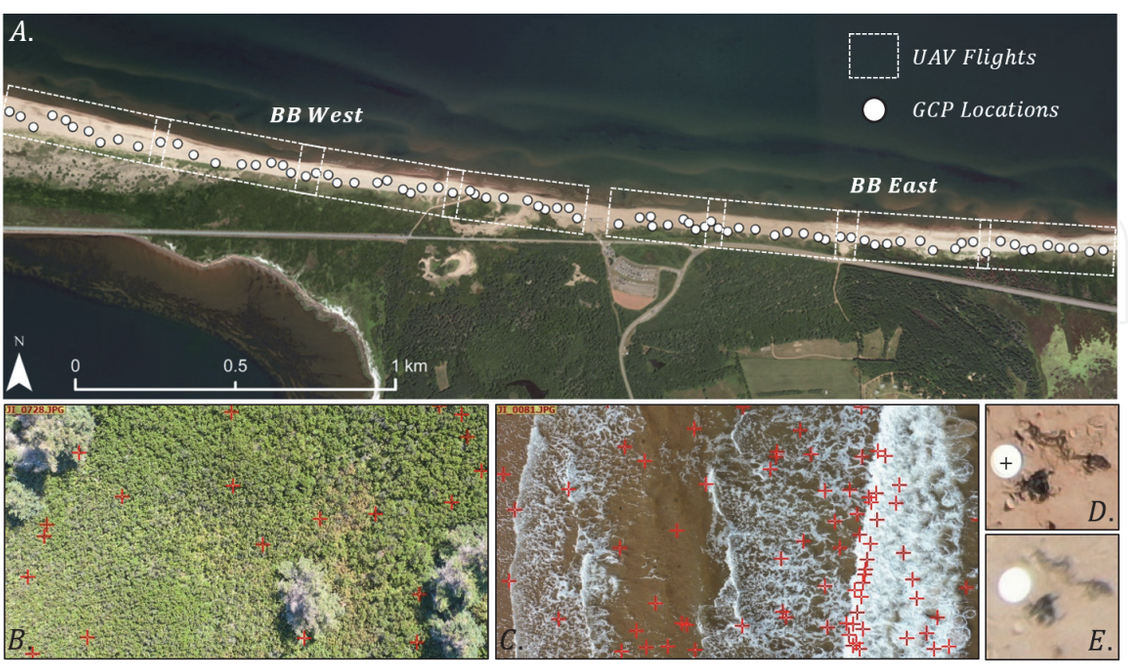


Figure 4.
UAV flight and GCP locations for the Brackley Beach (BB) east and BB west surveys (A). Quality control measures were taken during post-processing including removing photos that generated a limited number of ATPs, typically occurring in areas of homogenous vegetation or prominent peaked vegetation (B) and breaking waves in the nearshore (C). Also, only GCPs that were clearly visible and non-deformed were selected (D) while all others were left unmarked (E) in order to improve accuracy during geo-referencing.

removal if elevated error values are recorded. Common causes of error can include GPS survey (e.g., limited number of satellites or line of sight), pedestrian interference during UAV flights, or user identification error during post processing.

Images of all connected flight grids were collectively processed (i.e., BB West and BB East) using the commercial SfM software Pix4D. Alternative SFM software including Agisoft Metashape [36, 39, 40, 42–45] and Fledermaus v-7 [38] have been previously used and described. The remainder of this section will focus on the general Pix4D workflow used in this study. Initially, a target number of 10,000 ATPs were generated from each overlapping image. Next, Automatic Aerial Triangulation (AAT), Bundle Block Adjustment (BBA), and camera calibration were optimized for all images. Uncalibrated cameras, a result of errors in the internal (e.g. vibrations) or external (e.g., position and orientation) camera parameters, were deactivated to remove potential topographic deformation during point cloud generation.

Furthermore, flight lines on the periphery of the survey grid had difficulty finding a sufficient number of ATPs due to areas of homogenous vegetation (**Figure 4B**), selecting prominent features such as treetops from multiple angles (**Figure 4B**), or breaking waves in the nearshore (**Figure 4C**). As a result, severe over- or under-estimation of the surface can occur by misclassifying reference elevation values. In an attempt to reduce survey error, images were clipped to the primary area of interest (i.e., the beach-dune zone). This ensured an optimal number of ATPs present in each image and removed potential edge or 'bowl' effects that can distort the point cloud in areas away from the GCP locations [40]. Next, GCPs that were clearly visible in the flight images were zoomed into and marked at their centroid (**Figure 4D**) to ensure proper pixel selection. GCPs that were blurry (**Figure 4E**), warped, displayed limited contrast, or not entirely visible were not selected because un-proper pixel selection can also introduce error during geographic transformation. Marked GCPs were then used for geographic conversion resulting in a vertical RMSE of 0.028 and 0.021 for BB West and East, respectively.

3.2 DSM and DTM generation and environmental uncertainty

Following initial processing, a point cloud was generated and consisted of 2.65×10^{-8} points with a density of ~2000 points per m^2. The point cloud was classified using Pix4D's predefined class groups including ground, road surface, high vegetation, building, and human made objects, in order to improve DTM filtering. Point interpolation was completed using an inverse distance weighting (IDW) approach to generate a universal DSM (i.e., retaining all elevational classes) and filtered DTM (i.e., retaining only the ground elevation class) at a 1 m × 1 m resolution for direct comparisons to the pre-SD LiDAR DTM.

Prior to measuring topographic changes between surfaces, an initial assessment of the quality of the LiDAR DTM and UAV DSM and DTM displayed significant irregularities (**Figure 5A**). For instance, the LiDAR DTM was generated using green laser that can penetrate up to 5 m depth and full wave form infrared laser that can penetrate the vegetation canopy. This provides a fully integrated bathymetric and topographic surface transitioning from the nearshore—to backshore zones (**Figure 5A**). SfM is not able to penetrate the water column and has difficulty measuring ground points in vegetated areas. As a result, the SfM DSM captures noise above the surface that is associated with wave breaking and run up in the nearshore and foreshore zones (**Figure 5A** and **B**). In the backshore, the vegetated crest and lee slope is overestimated on average by ~0.5–1 m (**Figure 5A**) and represents variability in vegetation density and canopy height (**Figure 5B**).

Alternatively, the standard Pix4D DTM filtering method almost completely removed the foredune in areas that recorded significant scarping. **Figure 5A** shows

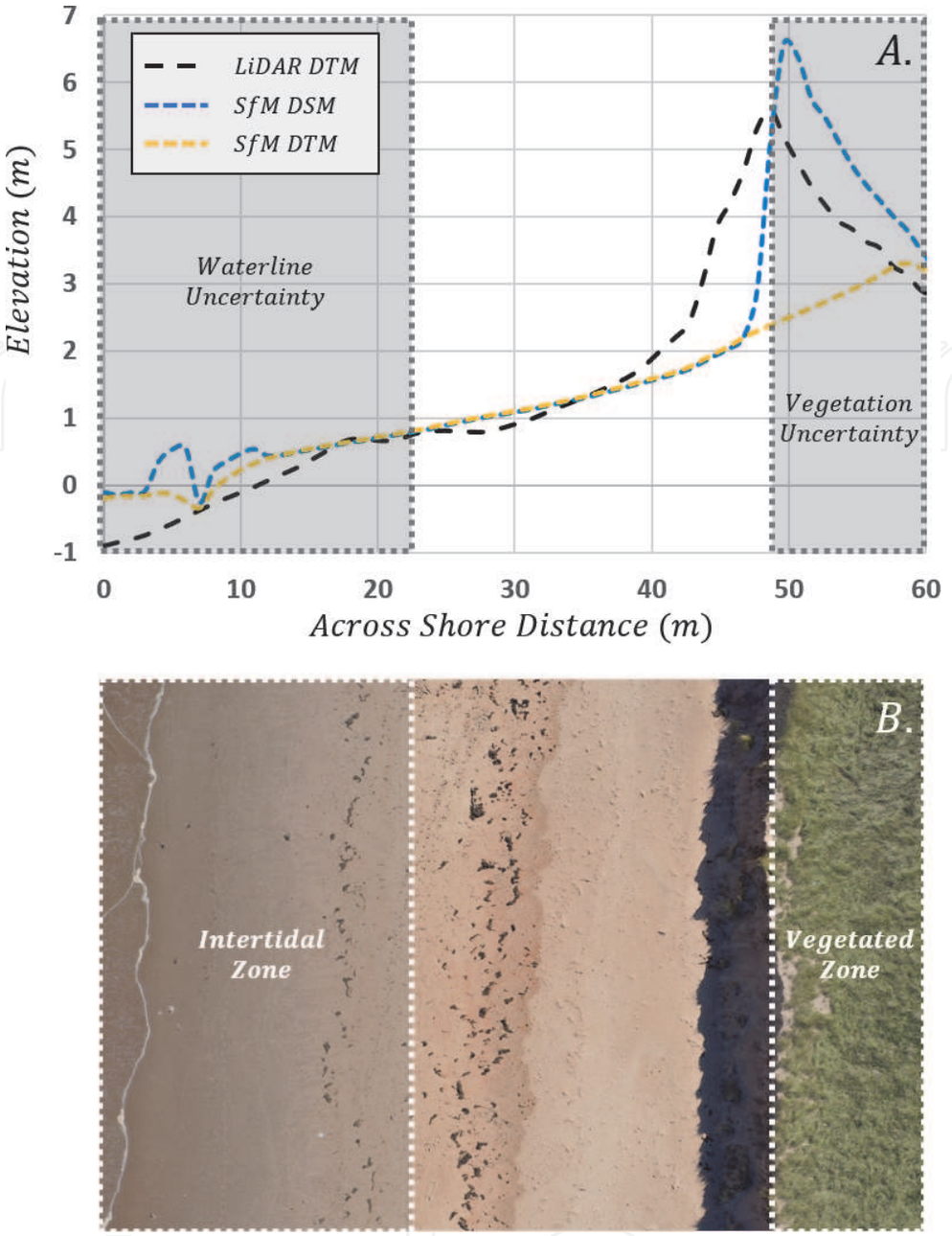


Figure 5.
Across shore profiles comparing the pre-storm Dorian (SD) LiDAR DTM and post-SD UAV DSM and DTM (A). Inconsistencies occur in the UAV surveys due to over-estimation of elevation values due to environmental uncertainties including the waterline (A) in the intertidal zone (B) and vegetation (A) in the vegetated back dune zone (B). Also, under-estimation of elevation values occurred due to over-filtering of the UAV DTM has almost entirely removed the foredune following SD.

a profile that was taken from a highly eroded foredune at BB East. Notice, only a small crest remains visible more than 2 m below and 10 m landward of the dune crest measured by the LiDAR DTM (**Figure 5A**). The removal of the foredune from the UAV DTM is indicative of over-filtering, not storm erosion. While good agreement exists between the SfM DTM and DSM over the non-vegetated upper beach surface (**Figure 5A** and **B**), the DTM filtering method could not resolve significant breaks in slope. Therefore, our UAV DTM was not capable of quantifying topographic changes associated with a distinct scarped foredune and will not be used for our post storm measurements.

To limit the environmental uncertainty associated with the UAV DSM, and to create a repeatable survey methodology, topographic change measurements must be confined to areas not affected by potential error introduced by water or

vegetation. Difficulty arises when demarcating a seaward boundary due to the fluctuation of the water line in the intertidal zone (**Figure 5B**). The higher high water (HHW) line, 0.8 m above mean sea level MSL [49], or average of the highest annual tide levels was chosen as the seaward boundary. The HHW line is typically above the fluctuating water line and provides a repeatable method to measure spatially comparable topographic changes through time, regardless of the yearly, monthly, or daily variability in tide ranges and cycles. The landward extent of the DSM was limited to the foredune scarp because it marks the boundary between non-vegetated and vegetated surfaces, post-SD (**Figure 5B**). By removing significant environmental uncertainties associated with the water and vegetation line, we improve our confidence in monitoring topographic changes occurring between the pre-SD LiDAR DTM and post-SD UAV DSM.

3.3 Volumetric change and uncertainty

Volumetric changes (ΔV (m^3); Eq. (1)) from pre- and post-SD are reported within the detectable range of the SfM derived DSM. Here, z_2 and z_1 represent the elevation of the surface in time series two (i.e., post-SD) and time series one (i.e., pre-SD), respectively, and $x\ (m)$ and $y\ (m)$ are the length and width of the raster pixels (p). To assess the accuracy of the ΔV measurements, the propagated error (PE (m)); Eq. (2)) reports the magnitude of error $(e(m))$ associated with both time series. Common e metrics include the RMSE [36, 38–40, 43, 44] and standard deviation error (σ, [50, 51]). Once the PE is determined, the volumetric change uncertainty (ΔVU (m^3); Eq. (3)) provides a universal error value associated with each p and allows for a range of uncertainty (i.e.,$\pm\Delta VU$) to be reported with the ΔV measurements (e.g., [50, 51]).

$$\Delta V = (z_2 - z_1)xy \tag{1}$$

$$PE = \sqrt{e_1^2 + e_2^2} \tag{2}$$

$$\Delta VU = n(p)PE \tag{3}$$

To minimize the uncertainty of the ΔV measurements, a threshold is applied to remove values of low magnitude topographic change. The magnitude of change, away from (i.e., $\pm$)PE, is measured using a statistical t-score approach (t; Eq. (4); [52]). A minimum 95% confidence level ($CL_{95\%}$; Eq. (5)) threshold of ~1.96, valid for large population sizes, is determined based on a two-tailed test that accounts for both negative and positive values that correspond to erosion and deposition, respectively. Absolute t values that exceed 1.96 are preserved representing areas of low uncertainty, while t values less than 1.96 are classified as zones of high uncertainty and removed from ΔV measurements.

$$t = \frac{z_2 - z_1}{PE} \tag{4}$$

$$CL_{95\%} = |t| \begin{cases} for & |t| > 1.96 \\ else & \varnothing \end{cases} \tag{5}$$

4. Results

Topographic changes, measured between the pre-SD LiDAR DTM and post-SD UAV DSM, display high magnitude and continuous erosion that mark the foredune

scarp along BB (**Figure 6A** and **B**). The scarp line consistently eroded into the seaward base of the foredune by >1 m, with higher magnitude erosion of the frontal section of the foredune of over 4 m recorded at eastward extent of the BB East survey (**Figure 6B**). Relatively low magnitude deposition of sediment of 0.2–0.4 m is observed in discontinuous areas of the beach, becoming more prominent at BB west. Despite these areas of significant erosion or depositional changes, 42% of BB (**Figure 6A** and **B**) is classified as a zone of uncertainty (i.e., below the $CL_{95\%}$ threshold). Low magnitude topographic changes of >-0.11 and <0.11, corresponding to a $|t|<1.96$, often mark an area of transition between sediment eroded from the foredune and deposited onto the beach. This area of transition or slope relaxation is typical of a 'winter' or flattened beach profile following storm events and was observed over the entirety of BB (e.g., **Figures 2** and **3B**).

Post-SD, a total volume change (ΔV) of $-11{,}004$ m^3 and volume change uncertainty (ΔVU) of ± 4704 m^3 was recorded (**Table 1**). High magnitude erosion, accounting for 49% of the detectable surface (**Table 1**), is the primary geomorphic change driver; however, this is associated with significant ΔVU accounting for 42% of the cumulative volume change value. To reduce the uncertainty associated with low magnitude elevation changes, the topographic change threshold ($CL_{95\%}$) was applied. As a result, ΔV remained similar at $-11{,}323$ m^3 but ΔVU was reduced to ± 2659 m^3 (**Table 1**). Notice that the higher magnitude erosional values now represents 57% of the $CL_{95\%}$ surface and ΔVU is reduced, accounting for only 23% of the cumulative volume change. Furthermore, after applying the topographic change threshold the observational area was reduced by 43% and ΔVU by 54% (**Table 1**). By accounting for the uncertainty introduced by the survey error, and associated with low magnitude elevation changes, we have systematically reduced ΔVU and improve our confidence in reported volume changes post-SD.

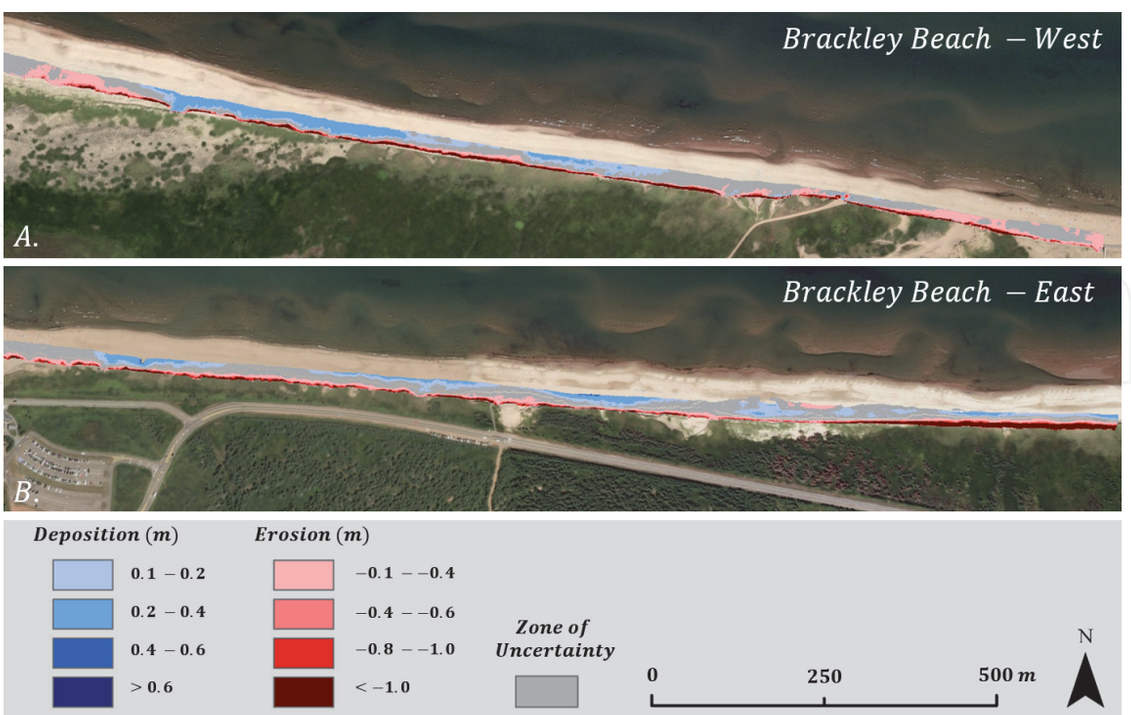


Figure 6.
Elevation changes at Brackley Beach West (A) and East (B), measured from the pre-SD LiDAR DTM and post-SD UAV DSM. A high magnitude and continuous erosional scarp is visible (i.e., in dark red) along the beach-dune boundary with the highest magnitude change occurring at the eastern extent of Brackley Beach East (B). Lower magnitude deposition (i.e., in blue) was observed to develop intermittently on the upper beach surface, becoming more continuous at Brackley Beach West (A).

	Observed	$CL_{95\%}$
Erosion (m^3)	−15,975 ± 2349	−15,201 ± 1509
Area (km^2)	0.038 (49%)	0.025 (57%)
Deposition (m^3)	4971 ± 2354	3878 ± 1149
Area (km^2)	0.039 (51%)	0.019 (43%)
Total change (m^3)	−11,004 ± 4704	−11,323 ± 2659
Total area (km^2)	0.077	0.044

Table 1.
Observed and threshold ($CL_{95\%}$) volume change (ΔV), volume change uncertainty (ΔVU), and area are reported for all erosional, depositional, and total change surfaces.

4.1 Alongshore variability

Alongshore, the eastern extent of the BB survey recorded the highest magnitude topographic change. This is particularly evident in areas that experienced erosion of the full-frontal section of the foredune (**Figure 7A** and **B**). In these locations, the scarp line forms at or behind the former crest line, leading to slope failure,

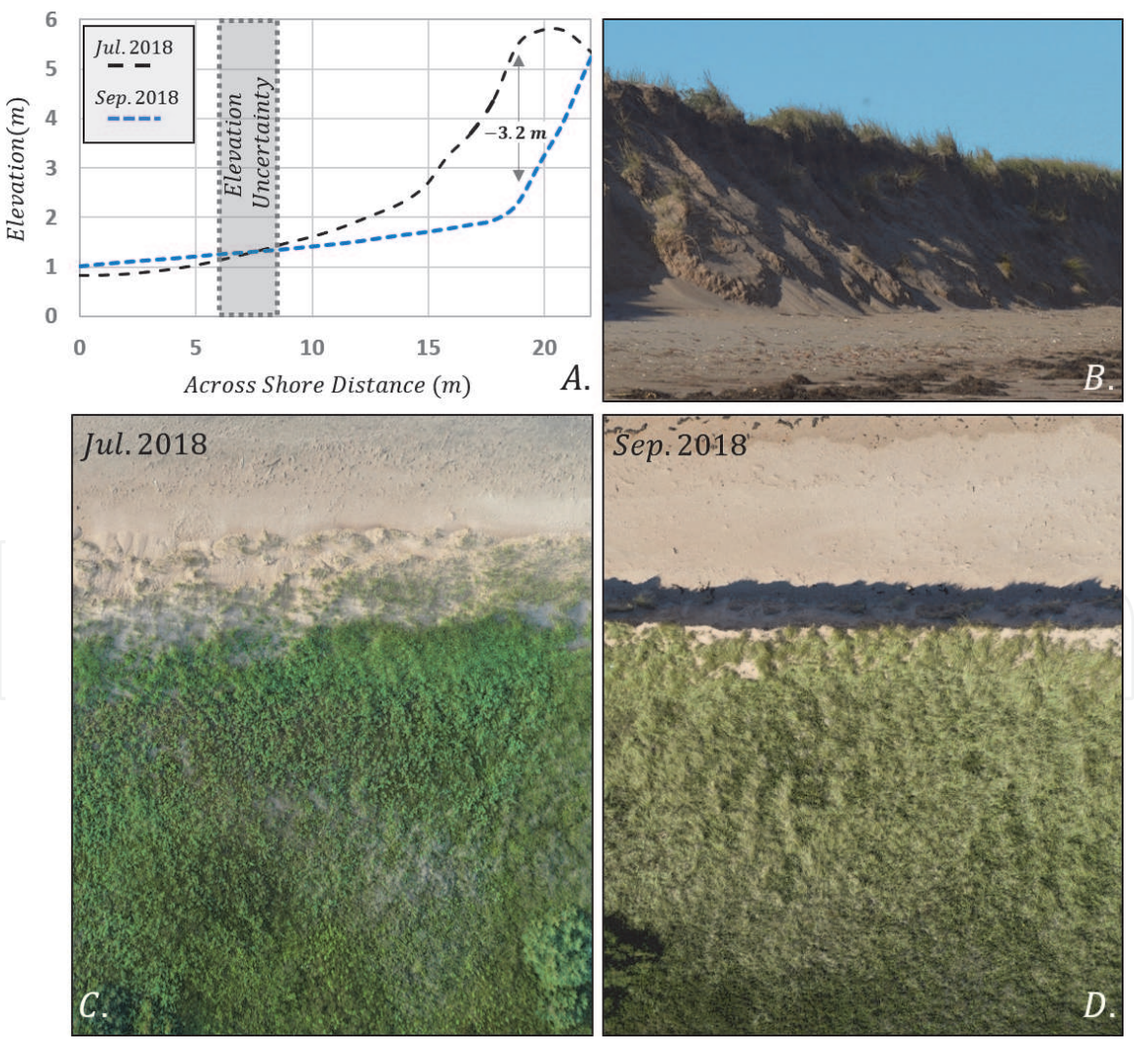


Figure 7.
A topographic change profile sampled from Brackley Beach (BB) east was measured from the pre-storm Dorian (SD) LiDAR DTM and and post-SD UAV DSM (A) BB east experienced significant scarping that eroded the frontal section of the foredune and lead to large volumetric losses (A and B). Aerial UAV images from pre-SD (C) and post-SD (D) show the removal of the stoss slope and formation of a steep scarp at the former crestline. Images from pre-SD (C) and post-SD (D).

significant downcutting and volumetric loss (**Figure 7A** and **B**). Only a small proportion of this eroded sediment was deposited on the upper beach surface suggesting that the majority of the sediment was moved further seaward, beyond the detectable range of our SfM DSM. Pre-SD, UAV images from July 2019 (**Figure 7C**) show a sparsely vegetated stoss slope extending ~10 m seaward of the dune crest. Post-SD, UAV images from September 2019 show the stoss slope has been entirely eroded leaving behind a steep scarp face formed at the crest line (**Figure 7B** and **D**). The foredunes in this area consistently displayed stoss slopes exceeding the angle of repose for dry sand ~>34° and appeared to be temporarily maintained by surface moisture post-SD. Additional slumping of the surface is expected and may lead to further instability and reduction of dune height at the eastern extent of BB East.

The mid and western sections of BB recorded a continuous ~1–2 m scarp at the base of the stoss slope, resulting in lower volumetric losses from the foredune in these areas (**Figure 8A** and **B**). At BB West, the transition between erosion and deposition occurs much closer to the dune toe, compared to BB east. Also, sediment deposition in this section of BB (**Figure 8A** and **B**) contained a high proportion of the volume eroded from the foredune (**Figure 8A**). In July 2019, prior to SD, the stoss slope of the foredune typically extended ~13 m or more seaward of the crest (**Figure 8C**). Sediment accumulation was aided by the increased seaward extent of

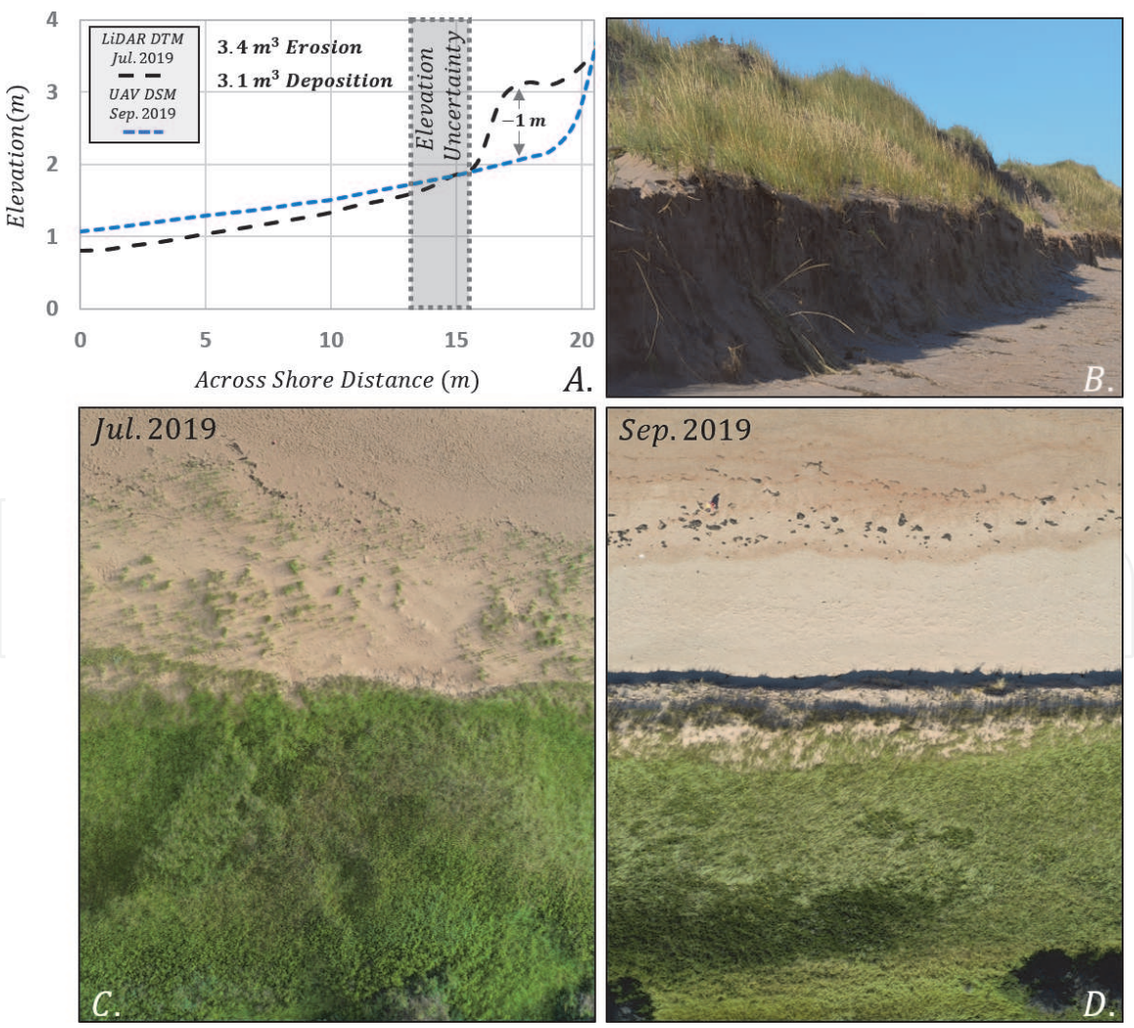


Figure 8.
A topographic change profile sampled from Brackley Beach (BB) west was measured from the pre-storm Dorian (SD) LiDAR DTM and and post-SD UAV DSM (A). BB west experienced scarping at the base of the foredune and removal of embryo dunes (A and B). Aerial UAV images from pre-SD (C) and post-SD (D) show the removal of seaward dune deposits leaving behind a low continuous scarp alongshore.

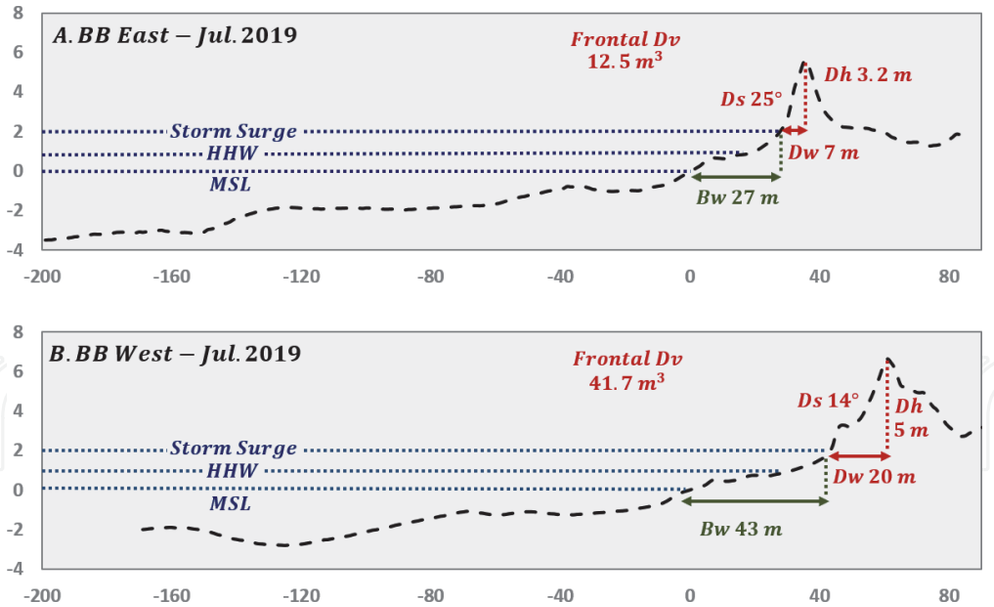


Figure 9.
Alongshore variability of antecedent (i.e., prior to the storm event) morphometry, measured form the LiDAR bathymetric and topographic survey at Brackley Beach (BB; A) east and BB west (B). BB east (A) displayed a higher sloping near shore, narrower beach (B_w) and dune width (D_w), lower dune height (D_h), higher slope (D_s), and lower (D_v) than BB west (B). These antecedent beach-dune metrics indicate that BB east was more vulnerable to storm erosion that resulted in higher magnitude scarping in this area of BB.

the vegetation during the summer months (**Figure 8C**) and promoted the intermittent growth of embryo dunes seaward of the established foredune (e.g., **Figure 8A** and **C**). Following SD in September 2019, the scarp line has eroded into the lower stoss slope and has removed any alongshore embryo dunes present pre-SD (**Figure 8D**).

The variability of storm impacts observed at BB were likely controlled by the antecedent morphology that existed prior to SD. From the LiDAR DTM, BB east was observed to have a higher nearshore slope and closer inner bar structure, in comparison to BB west (**Figure 9A** and **B**). This could have led to higher wave energy and erosive potential at BB East during SD, and stronger counter current moving sediment further seaward post-SD (e.g., **Figure 7A** and **8A**). Beach width (B_w) at BB East was also significantly narrower than BB West and likely would have increased the exposure of the foredune to wave run up, despite a lower storm surge level relative to the dune toe (**Figure 9A** and **B**). In comparison to BB West, a combination of foredune metrics including narrower dune width (D_w), shorter dune heights (D_h), higher dune slopes (D_s), and lower dune volumes (D_v) indicate that BB East was more vulnerable to storm induced erosion (**Figure 9A** and **B**). Foredunes that displayed a narrower D_w and high D_s at BB East experienced the highest magnitude of erosion resulting from major slope failures. While the foredune at BB West appeared to only lose a small proportion of the frontal D_v, a significant reduction of D_v at BB East could lead to further lowering of the foredune making this area of BB increasingly vulnerable to future storm events.

5. Discussion

UAV monitoring has allowed for the rapid assessment of Brackley Beach (BB), 11 days following Storm Dorian (SD). Projected 7–8 m significant wave heights and 1.2 m storm surge levels associated with SD resulted in a highly erosive post storm

surface, the majority of which occurred at the beach-dune boundary (**Figure 6A** and **B**). A total of ~11,000 m^3 of erosion was recorded between a pre-SD LiDAR and post-SD UAV survey (**Table 1**). This included the complete removal of embryo dune deposits and the formation of a continuous foredune scarp in the middle and western sections of BB (**Figure 8A** and **B**). At BB East, significant slope failure and high magnitude erosion of the frontal section of the foredune was observed (**Figure 7A** and **B**).

Despite a highly erosive post storm surface, a follow up field investigation in November 2019, or 2 months post-SD, observed the that the initial stages of dune recovery were already taking place. Evidence of the widespread remobilization of beach sediment by eolian processes was observed in the accumulation of dry ripple laden sediment deposits at beach-dune boundary, both across and alongshore (**Figure 10A**). This has resulted in the initial deposition of sediment into the dune scarp (**Figure 10B** and **C**) and ramps forming in areas of higher magnitude deposition (**Figure 10D**). Monitoring storm impacts can reveal initial topographic adjustments resulting from a single event; however, subsequent beach-dune responses can provide a broader understanding on the resiliency of sandy coastlines. Given the low cost, rapidity, and high resolution of UAV SfM surveys, researchers will increasingly have access to high resolution geo-spatial data sets to continuously monitor both short- and longer-term coastal dynamics.

Although UAV SfM research has increased significantly over the last few years, studies that have reported topographic or volumetric change from beach-dune systems are still limited [37, 38, 40, 44, 45]. In part, this has been due to the inherent difficulties in data collection, post-processing, and handling of survey



Figure 10.
Initial dune recovery was observed during a follow up field site assessment in November 2019, or 2 months following storm Dorian (SD). Alonshore, dry sediment has begun to accumulate at the beach-dune boundary (A). This has resulted in the initial accumulation of sediment at the dune scarp (B and C) and ramp development in areas of higher magnitude deposition (D).

artifacts (e.g., vegetation). This chapter has attempted to address some of these common challenges using basic quality control measures and handling of data uncertainties. In doing so, we were able to confidently quantify alongshore topographic and volumetric changes resulting from a storm event. Survey uncertainties in our post-storm measurements were mitigated due the implementation of quality controls to produce high accuracy (i.e., low RMSE) surface models from UAV surveys. Furthermore, environmental uncertainties were reduced in large part by the wave induced removal of vegetation from the beach dune boundary post-SD. While vegetation uncertainty did not significantly constrain our post storm measurements of the dune scarp, subsequent dune recovery studies will need to develop new strategies to handle uncertainty introduced by vegetation recolonization of the backshore zone.

The quality controls measures, discussed in Section 3, partially include data processing techniques that are unique to the Pix4D software. It is currently beyond the scope of this chapter and expertise of the authors to provide a comprehensive review of different SfM software. Therefore, the remainder of this discussion will focus on addressing survey and environmental uncertainties.

5.1 Survey and environmental uncertainties

UAV SfM surveys have proven to be highly accurate with RMSE values, typically <1o cm [36, 38–40, 43]. This level of accuracy is capable of monitoring topographic adjustments associated with storm impacts. However, the uncertainty of topographic change measurements should be reported especially when changes approach the same magnitude of the survey error. While the RMSE values are commonly reported, interpretation of how these values influence uncertainty in topographic change measurements are not. To address survey error, a previous study used RMSE as a threshold to monitor topographic change [44]. In this study, the RMSE value was 16 cm and only positive or negative values in exceedance of ±16 cm were reported. This method is effective at filtering data that could represent no change, but there still could be a high level of uncertainty associated with low magnitude changes. For instance, 17 cm of deposition recorded from a 1 m × 1 m pixel would result in a volume change (ΔV) and volume change uncertainty (ΔVU) 0.17 m^3 ± 0.16 m^3, respectively. Or in other words, 94% of the ΔV would be within the range of uncertainty. This indicates that interpreting the significance of low magnitude topographic changes should be done carefully and only after survey uncertainty has been reported and adequately addressed.

Results presented in this chapter limited survey uncertainty by applying a topographic change threshold ($CL_{95\%}$) that approximates to a minimum detectable range of 1.96 times the propagated RMSE value. Applying $CL_{95\%}$ effectively increased the confidence in ΔV measurements by filtering out small magnitude changes that are disproportionately responsible for high levels of ΔVU. For example, 42% of the total observable area of post-SD BB was classified as a zone of elevational uncertainty but, once removed, this only resulted in a change of total ΔV reported by 3% (**Table 1**). Furthermore, the ratio between ΔV and ΔVU dropped from 49 to 23% prior to- and after the$CL_{95\%}$ threshold was applied. It is important to note that ΔV below the $CL_{95\%}$ threshold, or within the zone of uncertainty, may represent actual change; however, to increase confidence in reported ΔV values it is important to systematically address survey uncertainty. This chapter has demonstrated that thresholding can be an effective approach to reduce topographic change uncertainties, but the most effective approach remains the quality of repeatable survey strategies and data processing (e.g., discussed in Section 3). For coastal studies, maintaining a high level of survey accuracy limits the areal extent and vertical range

of elevational uncertainty and will allow for low magnitude and morphologically significant topographic adjustments (e.g., dune recovery) to be observed through time.

Environmental uncertainties within UAV SfM data also pose a significant challenge as they are space and time dependent. Images taken at the water boundary often captures breaking waves, wave run up, or low contrast moist surfaces in the nearshore and foreshore zones. This can lead to insufficiencies in ATP generation during SfM processing [36, 37, 41] and inconsistencies on the seaward extent in which repeat topographic change measurements are taken. Previously, mean sea level (MSL; [45]) and the wet-dry line [44] have been identified as the observable extent of coastal DSMs. These provide a reasonable estimate of the average annual water line or the water line at a particular time but can become inconsistent when monitoring spatially and/or temporally extensive surveys.

For instance, 2.5 km of post-SD BB was surveyed over a two-day period with approximately 4 h of surveying time per day. Considering the 6 h semi-diurnal (i.e., two high and low) tidal cycle at BB, variability of the across shore extent of the wet-dry line was captured during our alongshore survey. Beyond daily cycles, monthly and annual cycles effect the magnitude of the tidal range and can result in significant variability of the water line boundary during repeat surveys. This may introduce uncertainty when quantifying multi-temporal sediment budgets (e.g., ΔV) and beach metrics (e.g., beach width) as these values may be over- or under-estimated depending on unique spatiotemporal tidal patterns captured while surveying. Alternatively, this chapter used the HHW line as consistent elevation that is typically above the intertidal foreshore zone regardless of tide cycles and ranges. While this approach is conservative in constricting the seaward survey extent, it provides a repeatable methodology to limit environmental uncertainty at the water line boundary.

At the beach-dune boundary, perhaps the biggest challenge in producing repeat UAV surveys in sandy coastal systems is the presence and handling of vegetation. Vegetation can directly lead to over-estimation of surface elevation values in SfM DSMs or point clouds [41]. Furthermore, any topographic change values that have not removed vegetation would be inaccurate as they could represent either a change in vegetation density or canopy height at the seasonal scale or loss of vegetation following a disturbance [38]. Post-SD, elevated storm surge removed vegetation seaward of the scarp along BB and did not have a significant influence our ability to measure topographic change; however, following storm events or seasons, vegetation recolonization could constrain subsequent monitoring surveys during periods of high growth rates.

A UAV vegetation monitoring study at BB from July 2019 sampled vegetation density, almost entirely low profile (i.e., ~50–60 cm) *Ammophila breviligulata* (*Ab*), both across- and alongshore during the peak growing season [53]. Across shore (i.e., from the shoreline to the back dune zone), vegetation density tended to fluctuate between the vegetation line and dune toe, followed by a rapid increase in density up the stoss slope, before reaching 100% density near the crest (**Figure 11A**). Alongshore, the overall density between the shoreline and dune crest, sampled at every 10 m along BB, ranged from 10 to 60% (**Figure 11B**). Taking into account uncertainty introduced with the fluctuating water line, only a narrow band landward of the foreshore and seaward of the vegetation line would consistently be observable without error introduced by spatially and seasonally variant vegetation density patterns.

A high resolution SfM derived point cloud of ~2000 points per m^2 was produced from a preliminary UAV survey during July 2019 (**Figure 11B**). The high vegetation density during the peak growing season is evident in the backshore; however, a large number of 'bare earth' points are also visible (**Figure 11B**). An attempt to filter

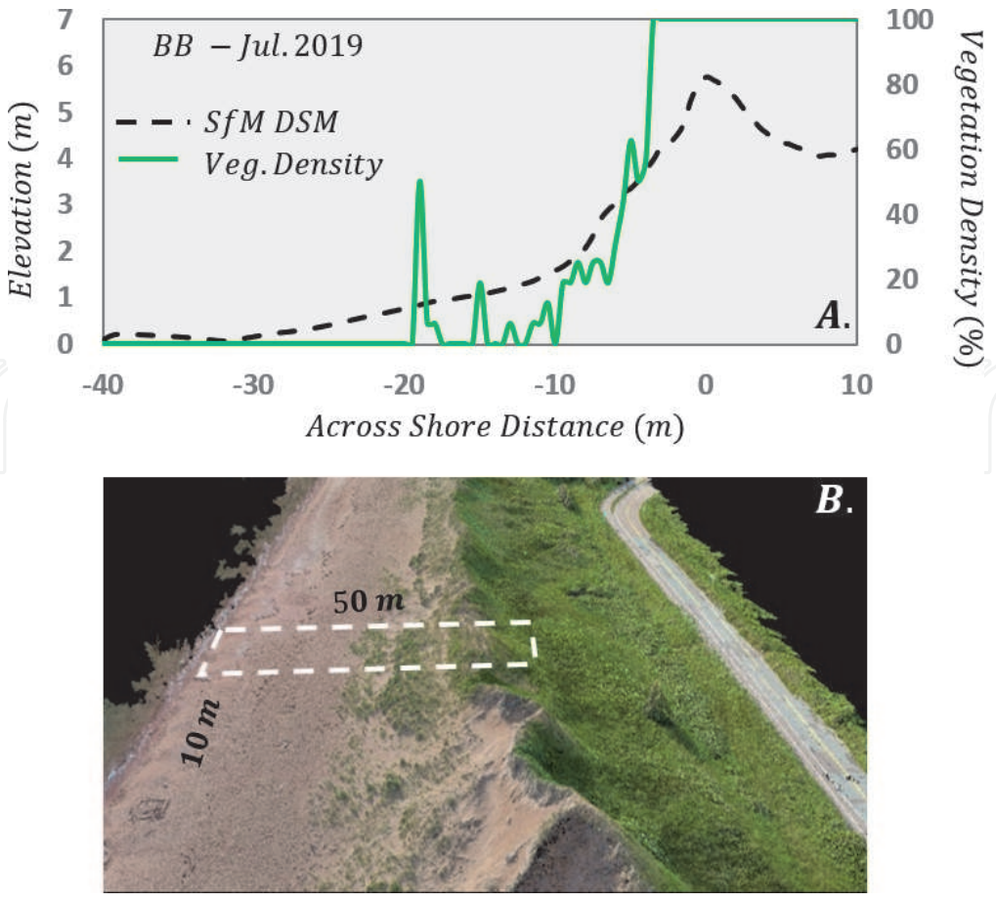


Figure 11.
An across profile and vegetation density, measured from aerial UAV photos taken at Brackley Beach (BB) in July 2019, show variable density at the seaward extent followed by rapid increase in density from the mid stoss slope to dune crest (A). The UAV SfM point cloud generated for this same section of BB, show variability in bare sand and vegetated points captured in the point cloud as you move landward from the sparsely vegetated beach-dune boundary to highly vegetated back dune zone (B).

the point cloud was completed in Pix4D and consisted of classifying and removing supra-surficial features and produce a 'bare earth' DTM. The standard Pix4D vegetation class, 'high vegetation', may be suitable for other prominent vegetation types (e.g., trees) but was not designed for and, therefore, unable to adequately classify and remove low profile vegetation that typically grows on the backshore (e.g., *Ab*; **Figure 11B**).

Vegetation filtering can be improved by applying algorithms that have been specifically designed for removing beach grasses. For example, a recent study [41] applied a vegetation filtering method originally designed to filter *Ab* from a TLS derived point cloud [51]. Results of this study show that sparsely vegetated foredunes can be effectively filtered from relatively low density SfM derived point clouds (i.e., ~100 points per m^2), but do not perform as well in areas of higher vegetation densities, relative to higher density point clouds (i.e., ~2000 points per m^2) produced from a TLS sensor. Vegetation is often intermittent at the beach-dune boundary, suggesting that point cloud filtering approaches, especially when applied to higher density SfM point clouds (e.g., **Figure 11B**), could accurately monitor low magnitude topographic changes associated dune building and recovery. In this regard, further studies are needed to test the capability of different vegetation filtering algorithms to remove variant patterns of backshore vegetation growth. Handling of vegetation remains problematic and, without using a suitable filtering method or quantifying the additional uncertainty that it may introduce, should not be included in topographic change measurements.

The density and variety of vegetation increases at BB moving from the crest landward. As a result, a significant reduction in the 'bare earth' points become problematic in these areas (**Figure 11B**). Vegetation filtering then becomes a less viable option. Although, these locations are less prone to low magnitude topographic changes, quantifying dune metrics (e.g., D_h or D_v) measured from UAV surveys would likely be inflated. Highly vegetated back dune areas are typically stable as they are protected from the wave, tidal, and wind processes that are actively shaping the seaward zones. These locations are likely to remain a 'zone of uncertainty' in UAV SfM surveys without significant vegetation removal or burial through blowout development, breaching, or overwash events.

Therefore, current UAV SfM applications for monitoring repeat topographic changes occurring in coastal systems are likely to be constrained to the backshore. The accuracy of UAV SfM data on unvegetated surfaces has been demonstrated and there is significant potential to increase the accuracy of sparsely vegetated foredune slopes by applying filtering algorithms (e.g., [41]). It is evident that challenges still remain in resolving water and vegetation boundaries; however, the benefits of UAVs are also clear as they provide an accessible cost-effective method to produce high resolution and spatially extensive surveys of sandy coastal systems. The number of UAV SfM monitoring studies in coastal systems are likely to increase in the coming years, but in order for these studies to confidently report topographic adjustments between the beach-dune boundary, addressing data uncertainties and improvements in vegetation filtering methods are needed.

6. Conclusion

This chapter has addressed common problems associated with UAV SfM research on sandy coastlines by presenting a methodology for survey and quality control measures, handling of uncertainties, and the interpretation of storm impacts. This introduction to basic geo-spatial techniques and considerations is aimed at coastal researchers who are developing UAV monitoring strategies. UAVs are becoming increasingly used to monitor beach-dune dynamics, so a systematic approach to address these issues are needed. This study has shown the ability of UAV SfM to accurately report the topographic adjustments of a sandy coastline that has been impacted by a storm event. However, it is also noted that our ability to confidently report these changes was aided in the removal of vegetation at the beach dune boundary. Post-storm recovery of the beach-dune system will be coincident with periods of vegetation growth and, thereby additional environmental uncertainties will be introduced.

Future studies can advance upon these current methodological considerations, particularly regarding the application of vegetation filtering algorithms to reduce environmental uncertainties and constraints. A review of current filtering techniques applied to UAV SfM point clouds, and specifically aimed at removing vegetation characteristic of the backshore, could determine to what extent these systems are capable of continuously monitoring topographic changes occurring at the beach-dune boundary. Using UAV SfM systems to accurately monitor subsequent foredune recovery are dependent on addressing the spatiotemporal uncertainties discussed in this chapter and resolving remaining limitations in handling backshore vegetation. As UAV SfM studies continue to increase in volume, it is critical that uncertainties are addressed in order to confidently monitor topographic adjustments resulting from storm impacts, post-storm recovery, and the longer-term resiliency of beach-dune systems.

Acknowledgements

The authors would like to thank Prince Edward Island National Park for permitting our field work at Brackley Beach, logistical assistance, and supplying of equipment. We would also like to thank CBCL Limited for supplying the baseline LiDAR survey used in this chapter. Finally, a special thank you to Phillipe Wernette and Jacob Lehner for their invaluable field assistance.

IntechOpen

IntechOpen

Author details

Alex Smith*, Brianna Lunardi, Elizabeth George and Chris Houser
School of the Environment, University of Windsor, Windsor, Ontario, Canada

*Address all correspondence to: absmith9@uwindsor.ca

IntechOpen

© 2020 The Author(s). Licensee IntechOpen. This chapter is distributed under the terms of the Creative Commons Attribution License (http://creativecommons.org/licenses/by/3.0), which permits unrestricted use, distribution, and reproduction in any medium, provided the original work is properly cited. CC BY

References

[1] Sherman DJ, Bauer BO. Dynamics of beach-dune systems. Progress in Physical Geography. 1993;**17**(4):413-447

[2] Shepard FP. Beach Cycles in Southern California. Washington, DC: Beach Erosion Board, Corps of Engineers; 1950

[3] Bascom WN. Characteristics of natural beaches. Coastal Engineering Proceedings. 1953;**4**:10

[4] Houser C. Synchronization of transport and supply in beach-dune interaction. Progress in Physical Geography. 2009;**33**(6):733-746

[5] Cowell PJ, Thom BG. Morphodynamics of Coastal Evolution. Cambridge, United Kingdom and New York, NY, USA: Cambridge University Press; 1994

[6] Houser C, Ellis J. Beach and dune interaction. Treatise on Geomorphology. 2013;**10**:267-288

[7] Wernette P, Houser C, Weymer BA, Everett ME, Bishop MP, Reece B. Influence of a spatially complex framework geology on barrier island geomorphology. Marine Geology. 2018; **398**:151-162

[8] Masselink G, Castelle B, Scott T, Dodet G, Suanez S, Jackson D, et al. Extreme wave activity during 2013/ 2014 winter and morphological impacts along the Atlantic coast of Europe. Geophysical Research Letters. 2016; **43**(5):2135-2143

[9] Davidson-Arnott RG. Conceptual model of the effects of sea level rise on sandy coasts. Journal of Coastal Research. 2005:**21**(6):1166-1172

[10] Houser C, Hamilton S. Sensitivity of post-hurricane beach and dune recovery to event frequency. Earth Surface Processes and Landforms. 2009;**34**(5): 613-628

[11] Kandrot S, Farrell E, Devoy R. The morphological response of foredunes at a breached barrier system to winter 2013/2014 storms on the southwest coast of Ireland. Earth Surface Processes and Landforms. 2016;**41**(14):2123-2136

[12] Houser C, Hapke C, Hamilton S. Controls on coastal dune morphology, shoreline erosion and barrier island response to extreme storms. Geomorphology. 2008;**100**(3–4):223-240

[13] Jewell M, Houser C, Trimble S. Initiation and evolution of blowouts within Padre Island National Seashore, Texas. Ocean & Coastal Management. 2014;**95**:156-164

[14] Jewell M, Houser C, Trimble S. Phases of blowout initiation and stabilization on Padre Island revealed through ground-penetrating radar and remotely sensed imagery. Physical Geography. 2017;**38**(6):556-577

[15] Hesp P. Foredunes and blowouts: Initiation, geomorphology and dynamics. Geomorphology. 2002;**48** (1–3):245-268

[16] Houser C, Wernette P, Weymer BA. Scale-dependent behavior of the foredune: Implications for barrier island response to storms and sea-level rise. Geomorphology. 2018;**303**:362-374

[17] Houser C, Wernette P, Rentschlar E, Jones H, Hammond B, Trimble S. Post-storm beach and dune recovery: Implications for barrier island resilience. Geomorphology. 2015;**234**:54-63

[18] Houser C, Barrineau P, Hammond B, Saari B, Rentschler E, Trimble S, et al. Role of the foredune in controlling barrier island response to sea level rise. In: Barrier Dynamics and

Response to Changing Climate. Cham: Springer; 2018. pp. 175-207

[19] Short AD, Hesp PA. Wave, beach and dune interactions in southeastern Australia. Marine Geology. 1982;**48** (3–4):259-284

[20] Bagnold RA. The nature of saltation and of 'bed-load'transport in water. Proceedings of the Royal Society of London. A. Mathematical and Physical Sciences. 1973;**332**(1591):473-504

[21] Namikas SL, Edwards BL, Bitton MC, Booth JL, Zhu Y. Temporal and spatial variabilities in the surface moisture content of a fine-grained beach. Geomorphology. 2010;**114**(3):303-310

[22] Hesp PA. A review of biological and geomorphological processes involved in the initiation and development of incipient foredunes. Proceedings of the Royal Society of Edinburgh, Section B: Biological Sciences. 1989;**96**:181-201

[23] Suanez S, Cariolet JM, Cancouët R, Ardhuin F, Delacourt C. Dune recovery after storm erosion on a high-energy beach: Vougot Beach, Brittany (France). Geomorphology. 2012;**139**:16-33

[24] Sallenger AH Jr. Storm impact scale for barrier islands. Journal of Coastal Research. 2000;**1**:890-895

[25] Stockdon HF, Sallenger AH Jr, Holman RA, Howd PA. A simple model for the spatially-variable coastal response to hurricanes. Marine Geology. 2007;**238**(1–4):1-20

[26] Houser C, Mathew S. Alongshore variation in foredune height in response to transport potential and sediment supply: South Padre Island, Texas. Geomorphology. 2011;**125**(1):62-72

[27] Houser C. Alongshore variation in the morphology of coastal dunes: Implications for storm response. Geomorphology. 2013;**199**:48-61

[28] Dolan R, Hayden B. Storms and shoreline configuration. Journal of Sedimentary Research. 1981;**51**(3): 737-744

[29] Suter JR, Nummedal D, Maynard AK, Kemp P. A process-response model for hurricane washovers. In: Coastal Engineering. 1982. pp. 1459-1478

[30] Orford JD, Carter RWG. Mechanisms to account for the longshore spacing of overwash throats on a coarse clastic barrier in Southeast Ireland. Marine Geology. 1984;**56**(1–4):207-226

[31] Weymer BA, Houser C, Giardino JR. Poststorm evolution of beach-dune morphology: Padre island national seashore, Texas. Journal of Coastal Research. 2015;**31**(3):634-644

[32] Lorenzo-Trueba J, Ashton AD. Rollover, drowning, and discontinuous retreat: Distinct modes of barrier response to sea-level rise arising from a simple morphodynamic model. Journal of Geophysical Research: Earth Surface. 2014;**119**(4):779-801

[33] Cook KL. An evaluation of the effectiveness of low-cost UAVs and structure from motion for geomorphic change detection. Geomorphology. 2017;**278**:195-208

[34] Snavely KN. Scene reconstruction and visualization from internet photo collections [doctoral dissertation, PhD thesis]. Seattle, Washington, USA: University of Washington; 2008

[35] Westoby MJ, Brasington J, Glasser NF, Hambrey MJ, Reynolds JM. 'Structure-from-Motion' photogrammetry: A low-cost, effective tool for geoscience applications. Geomorphology. 2012;**179**:300-314

[36] Gonçalves JA, Henriques R. UAV photogrammetry for topographic monitoring of coastal areas. ISPRS

Journal of Photogrammetry and Remote Sensing. 2015;**104**:101-111

[37] Turner IL, Harley MD, Drummond CD. UAVs for coastal surveying. Coastal Engineering. 2016; **114**:19-24

[38] Scarelli FM, Sistilli F, Fabbri S, Cantelli L, Barboza EG, Gabbianelli G. Seasonal dune and beach monitoring using photogrammetry from UAV surveys to apply in the ICZM on the Ravenna coast (Emilia-Romagna, Italy). Remote Sensing Applications: Society and Environment. 2017;**7**:27-39

[39] Mancini F, Dubbini M, Gattelli M, Stecchi F, Fabbri S, Gabbianelli G. Using unmanned aerial vehicles (UAV) for high-resolution reconstruction of topography: The structure from motion approach on coastal environments. Remote Sensing. 2013;**5**(12):6880-6898

[40] Brunier G, Fleury J, Anthony EJ, Pothin V, Vella C, Dussouillez P, et al. Structure-from-Motion photogrammetry for high-resolution coastal and fluvial geomorphic surveys. Géomorphologie: relief, processus, environnement. 2016;**22**(2):147-161

[41] Guisado-Pintado E, Jackson DW, Rogers D. 3D mapping efficacy of a drone and terrestrial laser scanner over a temperate beach-dune zone. Geomorphology. 2019;**328**:157-172

[42] Laporte-Fauret Q, Marieu V, Castelle B, Michalet R, Bujan S, Rosebery D. Low-cost UAV for high-resolution and large-scale coastal dune change monitoring using photogrammetry. Journal of Marine Science and Engineering. 2019;**7**(3):63

[43] Papakonstantinou A, Topouzelis K, Pavlogeorgatos G. Coastline zones identification and 3D coastal mapping using UAV spatial data. ISPRS International Journal of Geo-Information. 2016;**5**(6):75

[44] Casella E, Rovere A, Pedroncini A, Stark CP, Casella M, Ferrari M, et al. Drones as tools for monitoring beach topography changes in the Ligurian Sea (NW Mediterranean). Geo-Marine Letters. 2016;**36**(2):151-163

[45] Guillot B, Castelle B, Marieu V, Bujan S, Rosebery D. UAV monitoring of 3-year Foredune Partial Recovery from a Severe Winter: Truc Vert Beach, SW France. Journal of Coastal Research. 2018;**85**(sp1):276-280

[46] Suo C, McGovern E, Gilmer A. Coastal dune vegetation mapping using a multispectral sensor mounted on an UAS. Remote Sensing. 2019;**11**(15):1814

[47] Sofonia J, Phinn S, Roelfsema C, Kendoul F. Observing geomorphological change on an evolving coastal sand dune using SLAM-based UAV LiDAR. Remote Sensing in Earth Systems Sciences. 2019;**2**(4):273-291

[48] Dalhousie Coastal Ocean Forecast System–DalCoast-HFX. Canada: Department of Oceanography, Dalhousie University. Available from: http://extrememarine.ocean.dal.ca/dalcoast/web/home.php

[49] Davies M. Geomorphic shoreline classification of Prince Edward Island. Report prepared by Coldwater Consulting Ltd. for the Atlantic Climate Adaptation Solutions Association (ACASA); 2011. p. 66

[50] Staley DM, Wasklewicz TA, Kean JW. Characterizing the primary material sources and dominant erosional processes for post-fire debris-flow initiation in a headwater basin using multi-temporal terrestrial laser scanning data. Geomorphology. 2014;**214**:324-338

[51] Smith A, Gares PA, Wasklewicz T, Hesp PA, Walker IJ. Three years of morphologic changes at a bowl blowout, Cape Cod, USA. Geomorphology. 2017; **295**:452-466

[52] Wheaton JM, Brasington J, Darby SE, Sear DA. Accounting for uncertainty in DEMs from repeat topographic surveys: Improved sediment budgets. Earth Surface Processes and Landforms. 2010;**35**(2): 136-156

[53] Lunardi B, Lehner JD, Houser C, Wernette PA, George E. Alongshore coupling of eco-geomorphological variables of a beach-dune system. In: AGU Fall Meeting, 9 AGU. 2019

IntechOpen